A vortex-element method for the calculation of waves and ship motions effects on propeller performance

Conference Paper · June 2024

CITATIONS
0

READS
10

1 author:

K.A. Belibassakis
National Technical University of Athens
250 PUBLICATIONS **3,711** CITATIONS

SEE PROFILE

Proceedings of the Thirty-fourth (2024) International Ocean and Polar Engineering Conference **www.isope.org**
Rhodes, Greece, June 16–21, 2024

ISBN 978-1-880653-78-4; ISSN 1098-6189

A vortex-element method for the calculation of waves and ship motions effects on propeller performance

Kostas Belibassakis
School of Naval Architecture & Marine Engineering, National Technical University of Athens, Greece

ABSTRACT

Ship propulsion performance in environmental conditions corresponding to moderate and more severe sea states is significantly affected due to ship motions and added wave resistance, as well as wind resistance and other factors. All the above cause significant additional energy losses that sometimes could drive the propulsion system at its limits, resulting in involuntary speed reduction and excessive fuel consumption. In this work the effects of wave-induced vertical oscillatory stern motion of the ship on the modification of propulsive thrust and efficiency are examined by means of Unsteady Vortex Element model used for the analysis of propeller(s) operating in the wake field of the ship, in conjunction with seakeeping analysis in regular and irregular waves.

KEY WORDS: Unsteady propeller analysis, Vortex Element Method, ship motion effects, wave effects

INTRODUCTION

Requirements and inter-governmental regulations for greening the waterborne transport have recently become very strict, especially concerning the development and demonstration of decarbonisation solutions and technologies in shipping, which can be used by shipowners to reduce Greenhouse Gas (GHG) emissions and fuel consumption by at least 55% before 2030 compared to 2008. In particular, propulsion technology for reduced pollution and environmental impact and response to the demand has been recognized to be an important factor concerning global warming and climatic change. On the other hand, the efficiency and economy of shipping against land and air transport, supports the growth of the fleets. The important role of shipping is clearly underlined by the fact that, today, about 90% of the world trade is being transported by ship. Thus, environmentally friendly technical solutions with reduction of exhaust gases are requested. Additionally, the increased competition in the field of maritime technology requires even more economical vessels. Therefore, optimization of ship propulsion performance in realistic conditions has become a central issue.

The technologies addressed to reduce the GHG emissions cover, except of the hydrodynamic design optimization related to minimization of hull resistance and optimization of propulsion efficiency (Papanikolaou 2022), the exploitation of Energy Saving Devices and renewable energy, from wind, waves and solar energy, ship electrification and improved management of the operational phase and of the on-board systems.

The wave resistance of a ship can be reduced by model testing and systematic application of modern design Computational Hydrodynamics tools. The frictional resistance of a ship may be reduced by injection of micro bubbles, using air films and polymers, super water repellent coatings, magneto hydrodynamics and surface shaping; details can be found in ITTC (2002, sec.8.5). Among several ESD technologies Air Lubrication Systems and Wind Assisted Propulsion are examined today for providing combined with design optimization an achievable solution; see, e.g., Spinelli (2022). In the case of WASP-equipped ships (Chu et al 2021) induced heel and leeway angles are expected to further affect the propeller behavior. Moreover, external factors such as ocean currents influence the actual flow on the propeller, and affect the behavior of the propulsion system. However, the ships rarely operate in calm sea, and in realistic sea states and adverse conditions additional components come into play, as e.g. added wave and wind resistance, as well as the effect of ship's stern motion on the propeller-hull interaction. Moreover, propellers and ship hulls get fouled. Several studies, see e.g., Muntean (2008), report achievable gains of ship energy losses of the order of 5% by exploiting accurate sensing to better control the propulsion train.

In this work the effects of wave-induced motions of the ship on the modification of propulsive thrust and efficiency are examined by means of Unsteady Vortex Element model used for the analysis of moving propeller(s) in the wake field of the ship. Information concerning the oscillatory vertical stern and propeller motion in waves can be provided by seakeeping analysis of the hull in regular and irregular waves. Results from the present hydrodynamic analysis, in conjunction with predictions of added resistance, are used to illustrate applicability in the case of a 82000DWT Bulk Carrier, investigating the benefits of of ship speed and engine RPM control from the point of view of optimizing ship's propulsive performance and reduction of energy losses. The present analysis could support the development of non-linear, multi-dof dynamical systems that will be used for the ship performance prediction in various sea states and wind/wave directions, as well as for the optimal design of the considered systems.

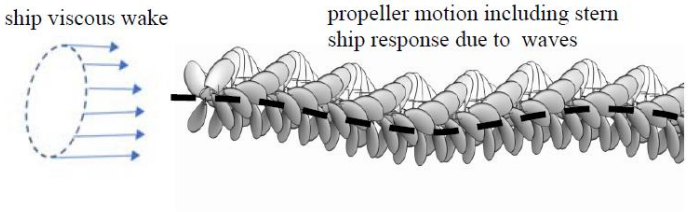

Figure 1. Unsteady proleller analysis including stern motion in waves

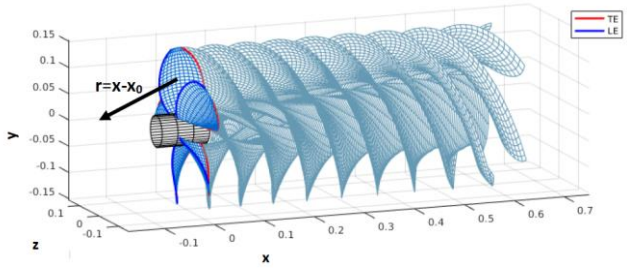

Figure 2. Modelling of propeler and trailing vortex sheets using surface vortex and source-sink elements.

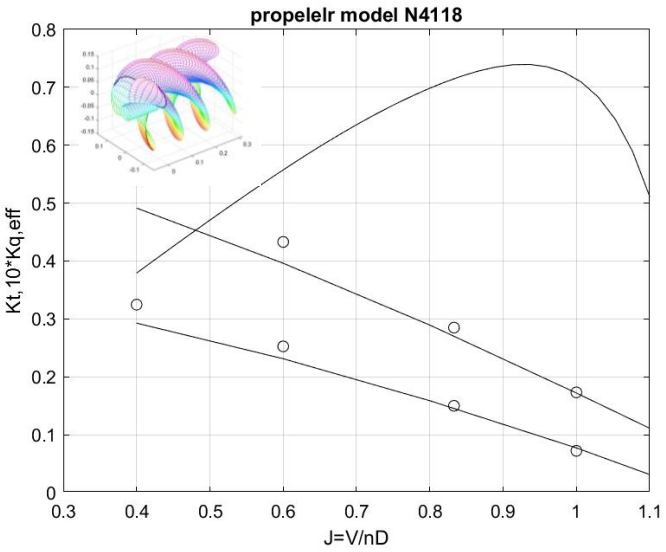

Figure 3. Open water characteristics of propeller N4118. Present model predictions are shown by using lines and experimental data by symbols.

UNSTEADY PROPELLER ANALYSIS

Assuming weak interaction between the propeller and the onset flow corresponding to the ship's wake, the unsteady propeller performance is treated in the framework of potential, lifting flow applications, modelling the vorticity generated by the propeller blades by trailing vortex sheets. The usual ways to reduce problems involving the Laplace equation for the propeller disturbance field to boundary integral equations is the direct method based on Green's representation formula, see, e.g., Kinnas (1996), Politis (2004), and methods based on singularity distributions; see, e.g., Belibassakis & Politis (1998).

In the present work the following representation is used to model the propeller disturbance velocity field:

$$\mathbf{u}(\mathbf{x}) = \frac{1}{4\pi}\int\limits_{S_B\cup S_C} \frac{\sigma\mathbf{r}}{r^3} dS(\mathbf{x}_0) + \frac{1}{4\pi}\int\limits_{S_B\cup S_W} \boldsymbol{\gamma}\times\frac{\mathbf{r}}{r^3} dS(\mathbf{x}_0), \qquad (1)$$

where $\mathbf{r} = \mathbf{x} - \mathbf{x}_0$, σ is surface source-sink distribution on the blade S_B and cavity S_C surface, and $\boldsymbol{\gamma}$ the surface vorticity on the blade and trailing vortex surface S_W. The solution of the problem is obtained in the time domain by the enforcement of the no-entrance boundary condition on the propeller blades and solid surfaces in the propeller frame of reference,

$$\mathbf{n}\cdot\mathbf{u} = -\mathbf{n}\cdot\mathbf{q}, \qquad (2)$$

where the total fluid velocity $\mathbf{w}$ is given by:

$$\mathbf{w} = \mathbf{q} + \mathbf{u}, \quad \text{with incident flow } \mathbf{q} = \mathbf{U} + \boldsymbol{\omega}\times\mathbf{r} + \mathbf{v}_s, \qquad (3)$$

with $\mathbf{U}$ and $\boldsymbol{\omega}\times\mathbf{r}$ denoting the components due to propeller translational and rotational speed, respectively, and $\mathbf{v}_s = (u_s, v_s, w_s)$ represents the disturbance of the incoming flow to the propeller due to ships viscous wake and any other factors. In this work we consider as additional components the effect of wave velocities on the propeller plane, in conjunction with the vertical stern motion due to ship heaving and pitching in waves, in the ship frame of reference; see Fig.1.

The simulation of the propeller hydrodynamic performance in the spatially varying inflow conditions due to ship's wake is based on the Vortex Lattice Method (Kerwin and Lee, 1978). The discretization consists of quadrilateral vortex element on the mean camber sufaces in conjunction with source-sink elements to model blade thickness and cavitation effects, as described in more detail in Belibassakis & Politis (2019). Trailing vortex sheets downstream the propeller blades are used to model circulation around the blade sections, which are determined as part of the solution by free wake analysis; see Fig.2. Also, wake models are alternatively used in order to reduce computation cost, in which the radial distribution of the hydrodynamic pitch angle is estimated from the main geometrical and hydrodynamic parameters; see, e.g., Politis and Belibasakis (1990). The vortex lines emanate from the trailing edge of each blade tangent to the local trailing edge bisector, and gradually deform to smoothly match the shape of the ultimate wake.

The numerical solution is obtained by a time-marching method where, at each time step, the velocity is computed from singularity distributions, and subsequently, the pressure is obtained from Bernoulli's equation; see also Katz & Plotkin (1991). The unsteady blade forces and moments, including the key blade thrust, $T_{,1}$, and torque, $Q_{,1}$, are calculated by pressure integration on propeller blades. For a specific mean value of the advance coefficient

$$J = U/(nD), \text{ where } U = (1-w)V_S, \qquad (4)$$

where V_S is the ship speed and $1-w$ denotes the mean volumetric wake fraction on the propeller disc (defined as the mean value of the axial propeller inflow), $n=\omega/2\pi$ denotes the propeller revolutions per second (ω is the propeller angular velocity), and $D = 2R$ is the propeller diameter, the blade thrust and torque coefficients are:

$$K_{t,1} = \frac{T_{,1}}{\rho n^2 D^4} \quad \text{and} \quad K_{q,1} = \frac{Q_{,1}}{\rho n^2 D^5}. \tag{5}$$

The corresponding propeller coefficients K_t and K_q, are obtained by summation taking into account the contributions by all blades and the phase difference of the corresponding load histories. As an example we consider the case of propeller model N4118. The basic dimensions of the above 3-bladed, unskewed propeller model with relatively thin blades are: diameter D=2R=0.3048m, pitch/diameter ratio P/D=1.077 (at 70% of tip radius), expanded area ratio 0.6, and the design value of the advance coefficient is J=0.833. The blade hub-tip ratio is 0.2, the blade section camber is NACA a08 and the thickness form NACA66mod. The present model predictions concerning the open water characteristics of the above propeller model, for which data are available (see, e.g. Kerwin and Lee, 1978 and Lee 1980), are shown in Fig.3 by using lines, and compared with experimental data shown by using symbols. Numerical predictions are obtained using a mesh of 15 x 7 elemens on each blade, in the spanwise and chordwise directions, respectively, depicted also in Fig.3, which is shown to be enough for convergence. Small differences observed in the torque coefficient are due to the viscous effects which are taken into accound by using a constant drag coefficient.

Next, the unsteady analysis of the propeller model is considered concerning its performance in the axial wake flow shown in Fig.3. Present model predictions are obtained using the same as before blade mesh and a time-step corresponding to 6deg propeller rotation. Calculated results concerning the unsteady hydrodynamic analysis of the above propeller model in non-cavitating conditions in the axial onset flow corresponding to the wake field shown in Fig.4, for the design value of the advance coefficient J=0.833, are presented in Fig.5. More specifically, the time-history of the thrust and torque coefficient of the key blade ($Kt_{,1}$ and $10Kq_{,1}$, respectively) are presented taking into account only the effect of the axial wake. Calculations are obtained using also viscous corrections based on empirical sectional drag coefficient for Re=10^6, from which the rotational speed of the propeller model is estimated as n=10.4rps and forward speed Vs=2.64m/s.

In this case the comparison between calculated and measured data concerning the mean propeller responses and the amplitude of the first blade harmonic are presented in Table 1. It is seen that the present numerical method provides good predictions especially concerning the mean propeller thrust and torque, while it leads to an overprediction of the blade frequency harmonics of the order of 10%, which is considered to be within acceptable limits concerning the examined case characterized by quite strong inhomogeneity.

Table 1. Responses of propeller model N4118

	model 0 harmonic	model 3 harmonic	experiment 0 harmonic	experiment 3 harmonic
Kt	0.145	0.075	0.150	0.068
$10Kq$	0.270	0.125	0.285	0.110

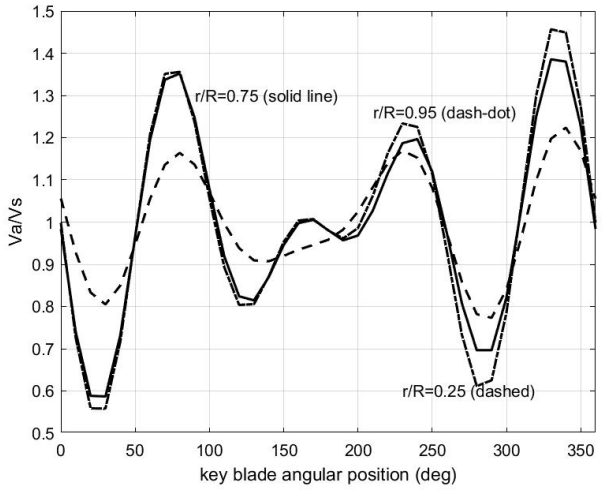

Figure 4. Axial wake distribution on the propeller disc representing ship's wake on the propeller disc of model N4118, for various representative blade radial positions during one revolution.

Application of the present vortex element method to other J values around the design value, J=0.833 of propeller model N4118, permits also the calculation of the mean Kt and 10Kq characteristics, from which the estimation of the derivative $\left[dKt/dJ\right]_{J=0.833} \approx -0.45$ is obtained for this propeller; see Fig.3.

Next, the problem of simulating the flow around a propeller undergoing more general motion, including the effect of the oscillatory vertical stern motion of the ship travelling in waves, while operating in the ship viscous wake, is considered. The propeller is considered operating in an unbounded fluid and the vertical oscillations of the propeller's origin is prescribed in the inertial (earth-fixed) frame of reference, as well as the instantaneous orientation of the axes of the body-fixed frame of reference, described by the rotation angles $\left(\theta(t), \psi(t), \chi(t)\right)$. In the present work, we consider a general path characterized by the propeller advance with the ship (steady translation), in conjunction with the induced vertical stern motion of the ship in waves, as e.g., predicted by

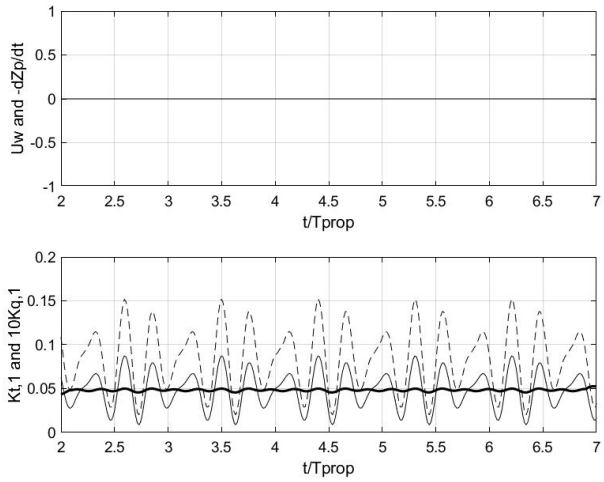

Figure 5. Calculated time-history of the thrust $Kt_{,1}$ (solid line) and torque $10Kq_{,1}$ (dased line) coefficients of the key blade during 5 revolutions, operating in the wake of Fig.4.

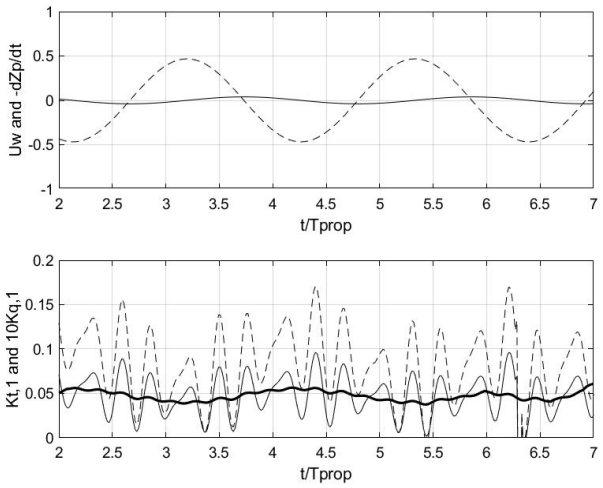

Figure 6. Calculated time-history of the thrust $Kt_{,1}$ and torque $10Kq_{,1}$ coefficients of the key blade during 5 revolutions with the additional effect of wave axial velocity (solidline) and vertical propeller motion (dashed line) plotted in the upper subplot.

seakeeping analysis. Also, the propeller is assumed to steadily rotate with angular velocity $\omega = 2\pi n$ about its own axis and performing pitching oscillations due to the motion of the ship in waves. Therefore, in the examined case we consider

$$X(t) = V_S t\,, \quad Y(t) = 0\,, \qquad Z(t) = \text{vertical stern motion}$$
$$\theta(t) = \omega t\,, \quad \psi(t) = \tan^{-1}\left(Z(t)/L\right), \qquad \chi(t) = 0\,.$$

Indicative results are presented in Fig.6 for propeller model N4118 operating at J=0.833, in the same as before conditions and in the wake distribution of Fig.4, taking in addition into account, except of the axial wake effect, also the oscillatory component of wave horizontal wave velocity component on the propeller disc and the vertical motion of the propeller. For simplicity, we consider harmonic waves of period $2\pi/\omega_w$=0.7sec (where ω_w is the wave frequency) with amplitude A=0.1R. Thus, the horizontal wave velocity incident on the propeller disc is

$$u_s(t) = -\left(gAk/\omega_w\right)\exp\left(-kd\right)\sin(\omega_e t)\,, \tag{6}$$

where d stands for the propeller submergence depth, $k = \omega_w^2/g$ is the deep water wavenumber, and $\omega_e = \omega_w + kU$ the encounter frequency in the case of head waves. Moreover, the velocity due to the vertical motion of the propeller, assuming the same amplitude A, is

$$w_s(t) = -\omega_e A\cos(\omega_e t)\,. \tag{7}$$

The above components are illustrated in the upper subplot of Fig.6 using solid and dashed lines, respectively. The calculated time histories of key blade trust and torque are plotted in the lower subplot of Fig.6 as obtained by the present method. It is clearly observed that the variation of $Kt_{,1}$ and $10Kq_{,1}$ is affected by the additional components $u_s(t)$ and $w_s(t)$ as illustrated in the lower subplot of Fig.6, where the low-frequency of oscillatory thrust response due to waves is also shown by using a thick solid line. The above analysis can be extended to take into account the above extra terms associated with the propeller oscillation in wave conditions characterized by a frequency spectrum using the ship responses; see also Belibassakis et al (2013).

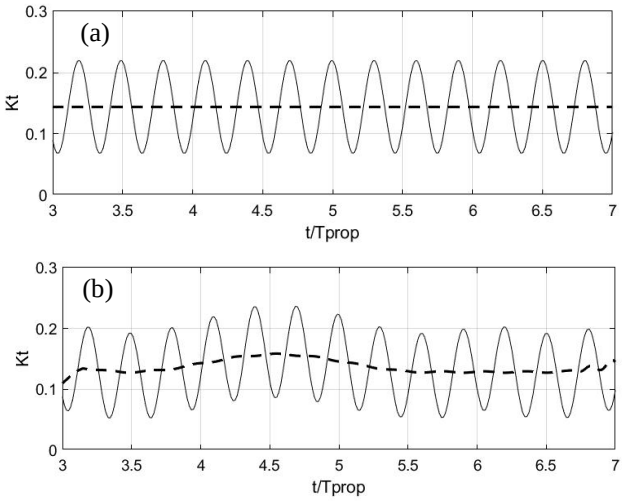

Figure 7. Total response concerning the thrust coefficient of the propeller N4119 in the wake of Fig.4 (a) without and (b) with the wave effects. The low frequency propeller response is shown by using dashed lines.

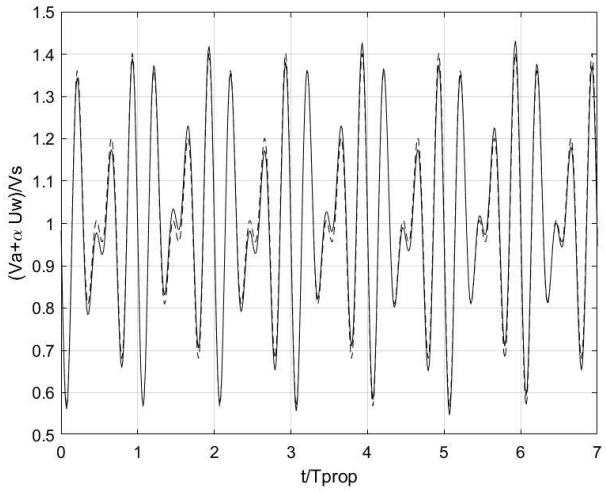

Figure 8. Axial velocity distribution on the N4118 propeller disc (dashed line) and modification due to the horizontal wave velocity (solid line) of period 0.7sec and wave amplitude A=0.1R.

Moreover, the total response from all blades concerning the thrust coefficient of the propeller operating at J=0.883 in the wake of Fig.2 without and with the above wave effects is shown in Fig.7. The observed rapid fluctuation corresponds to the blade harmonic frequency due to the ship wake effects, and the dashed lines in both subplots indicate the low frequency oscillation of the thrust response, which is induced by considering the additional wave effects. From Fig.7(b) we obtain that the amplitude of the low frequency response due to waves is of the order of 10% of the mean thrust value, and the corresponding thrust coefficient ranges in: $K_t = 0.145 \pm 0.015$.

A possible approach used for the prediction of the propulsive behavior of the ship and propeller in waves (see, e.g. Belibassakis & Filippas, 2022) is based on the application of surge equation with excitation by the waves and the propeller thrust, as follows

$$(1-t)T - \left(R + R_{AW}\right) + F_1 = \left(m + a_{11}\right)\ddot{\xi}_1 + b_{11}\dot{\xi}_1\,, \tag{8}$$

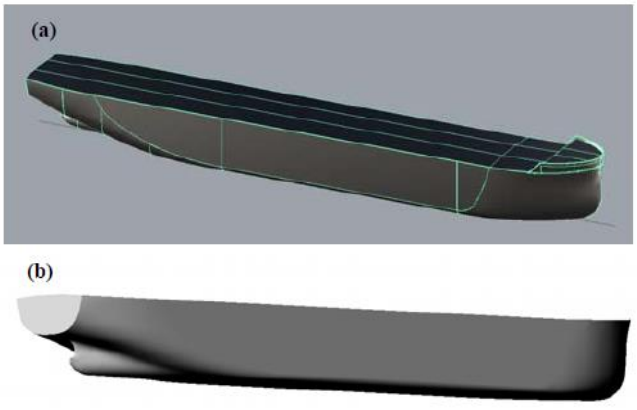

Figure 9. 3D plots of the BC hull studied with main dimensions: length L=229m, breadth B=32.28m, and deck height D_h=20m.

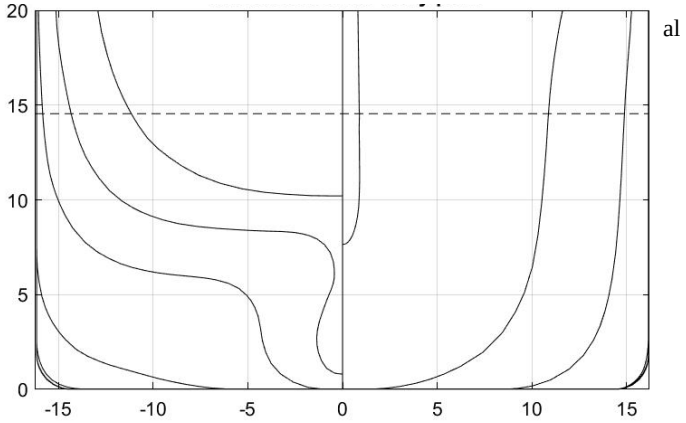

Figure 10. Body plan of the BC hull studied with main dimensions: length L=229m, breadth B=32.28m, and deck height D_h=20m. The scantling draft T_d=14.45m is shown by using a dashed line.

where T in the above equation denotes the propeller(s) thrust and 1-t the thrust deduction. Moreover, the components R, R_{AW} stand for the calm-water and the wave-added resistance, respectively, and F_1 the corresponds to the wave excitation forces along the ship long axis. In the right-hand side of the above equation, m is the ship mass and a_{11}, b_{11} the added mass and hydrodynamic damping coefficients in surge motion, respectively. Subsequently, by assuming that the ship surge oscillation $\left|\dot{\xi}_1\right| / U$ and the wave surge excitation F_1 / R are very small, a simplified method for considering the above effect, which facilitates its incorporation to ship propulsion dynamical systems, can be based on a quasi-steady approach using the open water propeller characteristics and the resistance requirements that are expressed by the parabolic curve:

$$\frac{K_t}{J^2} = \frac{R + R_{AW}}{\rho(1-t)\left(U + \alpha u_s(t)\right)^2 D^2} = C(t), \quad U = (1-w)V_S, \qquad (9)$$

where $u_s(t)$ is the horizontal wave velocity on the center of the propeller disc, as e.g., provided from Eq.(6). The above data, combined with the propeller K_t curve provides an estimation of the time-dependent

J- operation point, from which the propeller rps and the engine SHP can be estimated using the open water characteristics as follows

$$n(t) = \left(U + \alpha u_w(t)\right) / \left(J(t) D\right), \qquad (10)$$

$$SHP = \left(R + R_{AW}\right) V_S / PC, \quad \text{with } PC = \eta(t)\eta_H \eta_R \eta_S, \qquad (11)$$

where PC denotes the propulsion coefficient, $\eta(t)$ denotes the propeller open-water efficiency $\eta_H = (1-t)/(1-w)$ the hull efficiency and η_R the relative rotative efficiency at the given ship draft and trim condition, and finally η_S the shafting system efficiency.

In Eq.(9) α is a coefficient to be selected in order to include in the above simplified model also the effect of vertical oscillatory motion of the propeller $w_s(t)$ due to waves and the ship hull responses. Assuming that the two effects associated with $u_s(t)$ and $w_s(t)$ contribute similarly to the low-frequency oscillation of the propeller response in waves, the prediction of the wave and ship-response effects on the propulsion performance can be based on the quasi-steady approximation. In the example considered above concerning propeller N4118, the velocity is calculated from Eq.(6) to be : $\delta J = \left|\delta u_w\right| / U = 0.015$, and the amplitude of variation of the propeller thrust using the open-water characteristics is estimated to be: $\delta Kt = \left[dKt / dJ\right]_{J=0.833} \delta J \approx \pm 0.007$. Comparing the latter value with the result $\delta Kt = \pm 0.015$ derived by the unsteady propeller analysis in waves using the present Vortex Element Method (see also Fig.6), an estimation of the coefficient $\alpha = 2$ is suggested for the specific example. As an example in Fig. 8 the axial velocity distribution on the N4118 propeller disc due to ship's wake and its modification due to the horizontal wave velocity is shown by using solid line, for incident waves of period 0.7sec and amplitude A=0.1R.

Appropriate values for the above coefficient $\alpha(H_S, T_P)$ could be derived for other configurations and wave conditions by application of the present method to several cases of sea states, represented by the significant wave height Hs and peak period Tp of the corresponding wave spectrum and compare the result with the quasi-steady approximation, defined by Eqs. (9-11).

In the following, the case of a Bulk Carrier of DWT82000 will be examined and predictions of the propulsion performance in waves based on the above simplified approach will be presented, illustrating the applicability of the present model in realistic cases.

SHIP AND PROPELLER DATA

Main data concerning the ship studied, including 3D views of the hull surface are presented in Figs.9 and 10, corresponding to a Bulk Carrier vessel of DWT82000. The basic dimensions and data extracted from the 3d drawing are: Length L=229m, Breadth B=32.28m, Deck height D=20m (from keel). The scantling draft is T_d=14.45m, and in the full load condition the ship is without trim, with representative a value of the block coefficient is Cb=0.86. The calculated hydrostatic data are for this ship for drafts from 5m to T_d=14.45m are included in Table 2.

Moreover, the static stability diagram of the above BC, for the full loading condition T_d=14.45m, based on the value KG=11m concerning the vertical center of gravity (measured from keel) is presented in Fig.11. Using the fact that the ship is considered without trim, the long center of gravity coincides with the long center of buoyancy LCG=LCB=3.34m forward the midship section. Also, using the data concerning the vertical center of buoyancy KB=7.55m and metacenter position BM=6.24m, the the metacentric height is GM=2.79m for T_d=14.45m, as it is also shown in Fig.11 using dashed line.

Table 2. Hydrostatic data of BC hull based on the 3D model of Fig.7.

DRAFT	AREA	LCF	IMM.VOL.	DISPL.	I TRANS.	I LONG.	LCB	BM	KB	W.S.	BML
5.000	6124.7	8.358	29027.201	29832.068	490830.9	18854816.0	9.003	16.909	2.581	7725.6	649.6
6.000	6257.6	6.638	35200.207	36164.883	499831.2	20099132.0	8.789	14.200	3.093	8260.7	571.0
6.150	6301.9	6.007	36142.172	37131.465	503824.6	20516236.0	8.724	13.940	3.171	8364.7	567.7
8.000	6507.8	3.393	48026.371	49322.379	528500.1	22475176.0	7.663	11.004	4.138	9302.3	468.0
10.000	6795.3	-0.470	61401.586	63043.246	551774.1	25505300.0	6.182	8.986	5.199	10402.3	415.4
13.000	6968.6	-2.781	82119.227	84293.805	570800.5	27437406.0	4.114	6.951	6.790	11863.2	334.1
14.450	6998.2	-3.056	92245.125	94679.703	576056.8	27742860.0	3.342	6.245	7.551	12531.8	300.8

DRAFT	TP1	MCT1	CH.DISP.	CB	CWP	CM	CP	CB*	CWP*	CM*	CP*
5.000	62.778	886.601	240.077	0.82287	0.86812	0.98586	0.83467	0.78536	0.82855	0.98586	0.79662
6.000	64.140	933.229	192.425	0.82135	0.87607	0.98822	0.83114	0.79364	0.84652	0.98822	0.80310
6.150	64.594	950.816	175.035	0.82125	0.88066	0.98851	0.83080	0.79501	0.85252	0.98851	0.80425
8.000	66.705	1020.472	100.071	0.82222	0.89132	0.99117	0.82955	0.81212	0.88037	0.99117	0.81936
10.000	69.652	1145.198	-14.314	0.83183	0.92059	0.99293	0.83776	0.83064	0.91926	0.99293	0.83655
13.000	71.428	1230.061	-86.762	0.85467	0.94285	0.99456	0.85935	0.85454	0.94270	0.99456	0.85921
14.450	71.731	1243.553	-95.735	0.86366	0.94678	0.99511	0.86790	0.86359	0.94670	0.99511	0.86783

CB*,CWP*,CM*,CP* (IN CALCULATIONS LENGTH=L.P.P. AND BREADTH=BREADTH AT LOAD W.L.)

CB,CWP,CM,CP (IN CALCULATIONSLENGTH AND BREADTH = LENGTH AND BREADTH OF W.L.)

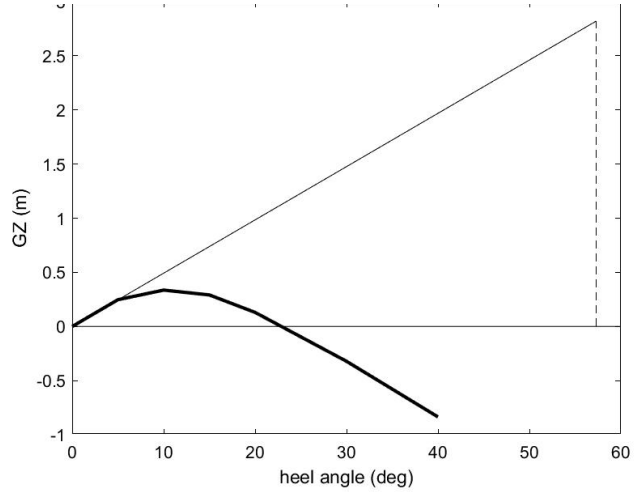

Figure 11. Stability diagram of BC hull for the scantling draft T_d=14.45m based on KG=11m from keel.

Table 3. Resistance (kN) of the BC hull of Figs.9,10 for full draft T_d=14.45m.

U(kn) / Hs(m)	10	12	13	14
1	0.5	0.2	0.1	0.1
2	9.6	7.0	6.0	5.4
3	51.3	42.2	38.4	35.1
4	160.8	149.1	143.4	138.8
5	342.8	344.9	345.8	344.1
R_{CW}	342.80	501.44	605.82	727.00

The ship is equipped with a Diesel main engine with MCR 9930 kW @ 90.4 rpm directly coupled to the propeller and the shafting system efficiency 98%. Also, from operational data the following ship speeds at the full loading conditions are identified: V_S=10-14kn. Available data from tank tests concerning the calm-water resistance in kN, for the above speed range, are included in the last column of Table 3. Also, data are available concerning the wake fraction: 1-w=0.36, the thrust deduction factor 1-t=0.25, and the relative rotative efficiency η_R=1.006, as obtained from test in the full load condition of the examined ship without trim.

The studied BC is equipped with a 5-bladed propeller of diameter D=6.95m, with expanded area ratio Ae=52% and pitch-to-diameter ratio P/D=0.77. The radial pitch distribution of the BC propeller, and data

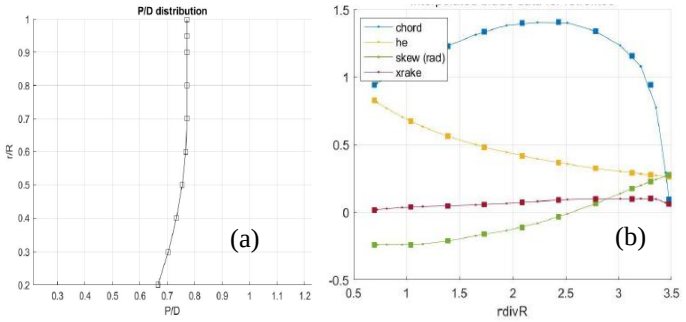

Figure 12. Pitch distribution of the BC propeller of D=6.95m, and data concerning the blade chordlength, skew and rake distributions used in the analysis. Presentation of the cortex element grid on the propeller blades and in the trailing vortex wakes.

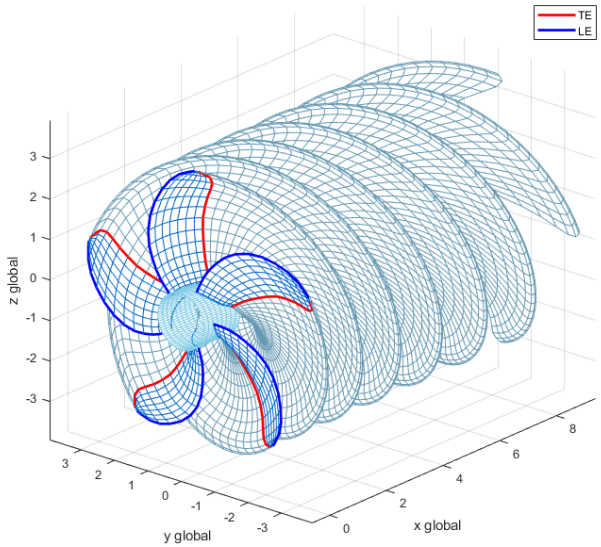

Figure 13. Vortex Element model used for the BC propeller analysis with a discretization of 15 spanwise by 7 chordwise elements per blade.

concerning the blade chordlength, skew and rake distributions are plotted in Fig.12, respectively. Based on the above data the open water characteristics of the propeller are calculated by the present vortex element method depicted in Fig.13, and the results are presented in Fig.14 by using solid lines and compared with results from CFD analysis used for verification, which are shown by using symbols. On the basis of the preceding analysis the predicted behavior of the propulsion system in calm water is presented in Fig.15 concerning the SHP-rpm data plotted on the engine diagram (Fig.15a) and the corresponding ship speed Vs-rpm data (Fig.15b). In this plot the propeller curve is indicated using red lines and for max RPM =90.4 we obtain Vs=14.54kn and SHP=8630 kW, with a margin of 13%.

In the same plots the operational data are also presented using symbols. The later data are fitted and the results are shown by using dashed blue lines, indicating on the average a difference in ship speed by approximately 1kn that could be due to effect of currents and an increase in SHP by 9% which could be due to weather conditions and other effects. The predictions are obtained using present model in conjunction with calm-water resistance data and hydrodynamic coefficients from self-propulsion tests.

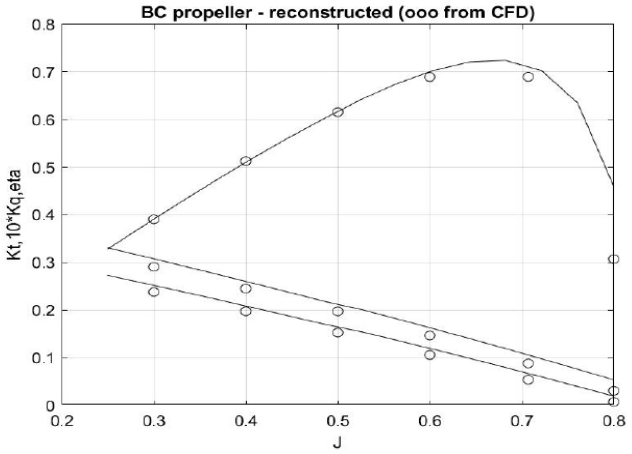

Figure 14. Open water characteristics of the BC propeller of Fig 11, as obtained by the present vortex element model using a discretization of 15 spanwise by 7 chordwise elements per blade.

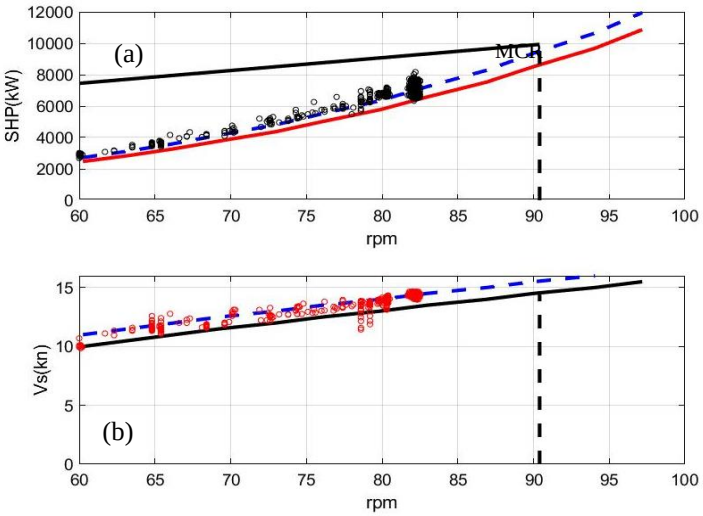

Figure 15. Behavior of the propulsion system based on the calm-water resistance for fill load draft T_d =14.45m without trim (shown by using solid line). (a) SHP-rpm diagram and (b) Ship speed -rpm diagram.

SEAKEEPING ANALYSIS

An important factor concerning ship operation in realistic sea-states is connected to ship dynamics, is added resistance in waves. This could also have a strong economical effect on ship exploitation. There are not many simple methods to obtain the added resistance in waves of a ship, and the validity of the results obtained by each method is not always good enough for different types of ships. In several works (see, e.g. Arribas 2007), available methods are studied and validated against seakeeping tests of some monohull models, focusing on head seas, that is usually the most severe situation concerning added resistance. The analysis shows that radiated energy method (Gerritsma & Beukelman 1972) is a method leading to relatively good-quality results in many cases. In the present study we employ the radiated energy method, as extended by Loukakis & Sclavounos (1978) for the prediction of head-to-beam seas, in conjunction with strip theory (Salvesen *et al* (1970)), for the calculation of the added resistance and the vertical ship motion at the stern; see also Lewis (1989,Sec. 3.4).

Table 4. Significant wave height and modal period for various sea states using the Bredschneider spectrum model.

Seastate	2	3	4	5	6
H_s(m)	0.3	0.9	1.9	3.3	5
T_p(sec)	6.3	7.5	8.8	9.7	12.4

Numerical results obtained concerning the responses of the BC hull studied are presented in Fig.16, for ship speed Vs=14kn, at full load draft without trim. In particular, the calculated RAO (modulus and phase) of heave and pitch motion are shown against the non-dimensional wavelength (λ/L). For the same condition and ship speed, the calculated response concerning the added wave resistance R_{AW} is plotted in Fig.17, for head incident waves β=180deg, where the calculated coefficient $WAR = R_{AW} / \left(\rho g A^2 B^2 / L \right)$ is shown, with A denoting the wave amplitude, and L,B are the ship length and breadth, respectively. The results concerning the calculated mean wave added resistance of the studied BC ship are listed in Table 3 for various ship speeds, from $V_S = 10 - 14$kn, corresponding to Froude numbers F=0.11-0.15, respectively, also in head waves (β=180°). In the case of irregular waves, we consider the responses of the system operating at various sea conditions labelled by a seastate index ranging from 1 to 5, corresponding to values of the significant wave height and modal period as listed in Table 4. For the calculations the Bretschneider model wave spectrum is used given by

$$S(\omega) = \frac{1.25}{4} \frac{\omega_p^4}{\omega^5} H_s^2 \exp\left(-1.25 \frac{\omega_p^4}{\omega^4} \right), \tag{12}$$

where the modal (peak) period $T_p = 2\pi / \omega_p$ is provided for various seastates in Table 4. A representative plot of the model spectrum for the model wave frequency spectrum concerning for Hs=3.3m, Tp=9.7s (sea state 5) is shown in Fig. 18.

The corresponding frequency of encounter ω_e is given by

$$\omega_e = \left| \omega - \left(\omega^2 / g \right) V_S \cos\beta \right| , \tag{13}$$

in terms of the absolute wave frequency ω, ships speed V_S and wave direction β. From Eqs. (12,13) the spectral density vs. relative frequency is obtained as follows,

$$S(\omega_e) = S(\omega) \left(1 - 2 \left(\omega V_S / g \right) \cos\beta \right)^{-1} , \tag{14}$$

where, as already discussed the Bretschneider model spectrum is used for $S\ \omega; H_S, T_p$. Assuming that the spectra of various quantities (wave velocity) can be calculated, short-term time series simulations, with reference to particular sea state $H_S, T_P; \beta$, can be obtained by considering the processes to be stationary characterized by the narrow band spectrum of the response(s). For example, in the case of horizontal wave velocity on the propeller

$$S_U\ \omega = \int_\theta \left| RAO_U\ \omega_e, \theta \right|^2 S\ \omega_e, \theta; H_S, T_p, \beta\ d\theta , \tag{15}$$

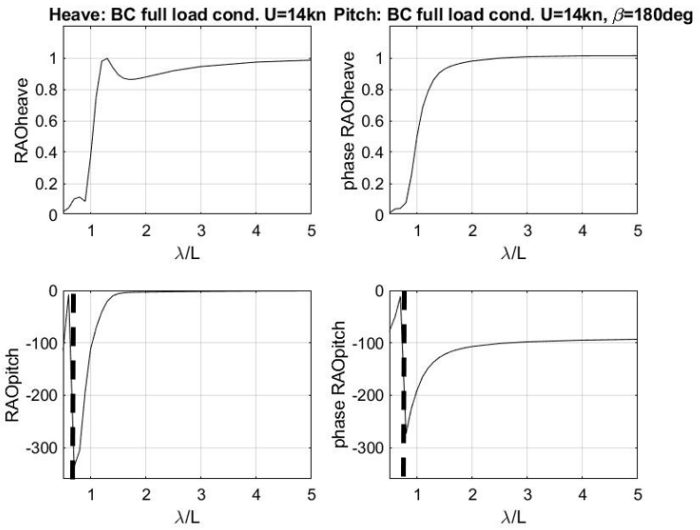

Figure 16. RAO (modulus and phase) of BC hull heave and pitch responses for Vs=14kn (F=0.15) against the non-dimensional wavelength (λ/L) for the full load condition (T_d=14.45m, without trim).

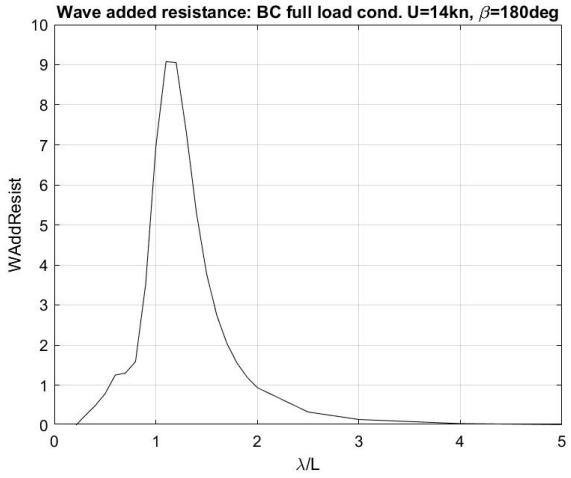

Figure 17. Calculated added wave resistance for the BC at full loading condition T_d=14.55m, Vs=14kn (F=0.15), and head incident waves β=180deg.

with $RAO_U\ \omega_e,\theta\ =\omega\ \omega_e\ \exp\ -d\omega^2\ \omega_e\ /g$ and d the propeller submergence depth. The stochastic simulation of wave velocities in the propeller plane is similarly treated. For simplicity, in the present study the wave spectrum is modeled as a unidirectional one, i.e. $S=S\ \omega_e;H_S,T_p\ \delta\ \theta-\beta$, representing long-crested seas. Subsequently, the random phase model (see e.g. Ochi 1998) and is applied to obtain a short-term time series of horizontal wave velocity on the propeller plane, as follows

$$u_w(t)=\sum_{n=1}^{N}U_n\cos\left(\omega_{e,n}t+\varepsilon_n\right), \tag{16}$$

where ε_n are random variables uniformly distributed in [0,2π). The horizontal wave velocity amplitudes are given by $U_n=\sqrt{2S_U(\omega_n)\delta\omega_n}$, and the set of discrete encounter frequencies $\{\omega_{e,n}\}$ are appropriately selected in order to cover the essential support of the spectra and to represent the energy distribution around the peak frequency. Similarly, the free surface elevation is modelled using the above random phase model as: $\zeta(t)=\sum_{n=1}^{N}A_n\cos\left(\omega_{e,n}t+\varepsilon_n\right)$, with $A_n=\sqrt{2S(\omega_{e,n})\delta\omega_n}$.

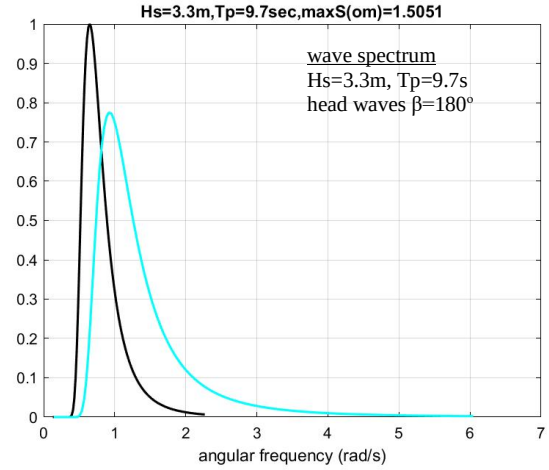

Figure 18. Wave frequency spectrum S(ω) for sea condition 5, using the Bredschneider model, normalized by its peak value. The same spectrum vs the encounter frequency for Vs=14kn is plotted by using cyan line.

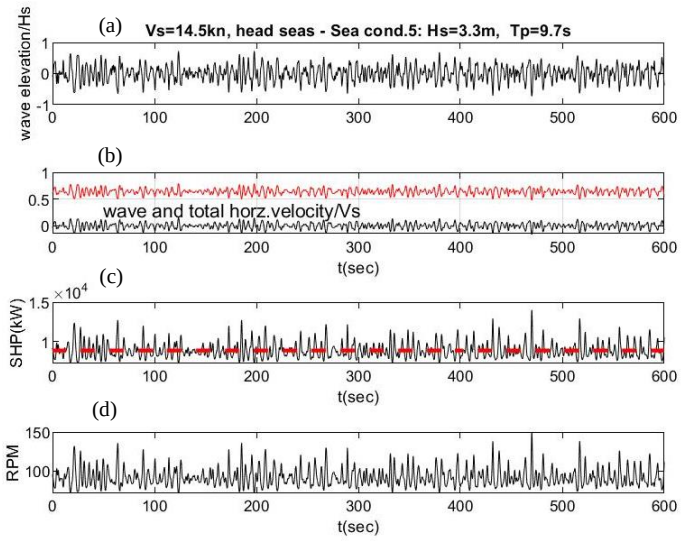

Figure 19. Simulated time series of (a) free-surface elevation and (b) horizontal wave velocity for the studied BC ship at full draft, travelling at speed of Vs=14kn (F=0.15) in head waves at sea condition 5. Dynamic simulation of propulsion system response concerning (c) SHP (kW) and (d) engine rpm.

Indicative results concerning the free-surface elevation and the horizontal wave velocity time series for the BC ship travelling at speed of Vs=14kn in head waves at sea condition 5 are shown in the top two subplots of Fig.19. More specifically in Fig.19b the horizontal wave velocity on the propeller plane $u_w(t)$ is shown using black line and the total velocity of the axial flow on the propeller $U+u_w(t)$ by using red lines, respectively. The dynamic simulation of propulsion system response concerning the SHP (kW) and the engine rpm is presented in the lower two subplots of Fig.19. Results are obtained by the present model, Eqs.(10-11) using $\alpha=2$. It is observed in this case that the

average SHP indicated by the red dashed line in Fig.19c is 8870kW which is 3% greater than the corresponding result in calm water, however, it is also observed that the peaks in the SHP and rpm time series exceed the MCR limit of the engine by 20%.

DISCUSSION

In the present work a seakeeping model based on strip theory is used to obtain predictions of the added wave resistance and ship motion data in waves, which are then used for simulating the system performance, taking into account the effects of wave orbital velocity and the vertical stern motion on the unsteady propeller analysis. The results derived by the above uncoupled (one-way) scheme, as presented in Fig.19 in the case of the studied BC ship, travelling at full draft with speed *V*s=14kn in head waves at sea condition 5, facilitate the cost-effective treatment of many similar cases required in realistic ship operation, supporting further applications, as for example, the development of digital-twin systems for optimum weather routing and decision support systems. An essential limitation of the present model is connected with the linearity assumptions of its main components, which makes its predictions less accurate in the case of large amplitude waves. Next steps include the comparison and verification of the present simplified model predictions against results obtained by fully-coupled methods based on sophisticated CFD models for specific selected conditions, and the calibration of the parameters for the enhancement of its efficiency.

CONCLUSIONS

In this study we have examined the effects of waves and wave-induced vertical motion at the stern of the ship on the propeller operational characteristics, obtained by means of a vortex element method for unsteady propeller analysis. Results, including predictions of the added wave resistance, obtained by strip theory and the radiated energy method, are then used to illustrate applicability to the case of an 82000DWT Bulk Carrier. The present analysis could facilitate development of ship monitoring decision support systems, integrated with engine and control systems, aiming to maximize operating performance. Future extension of the present work will focus on the elaboration of the present dynamical model to include additional factors, as e.g., currents and wind effects.

ACKNOWLEDGEMENTS

The present work has been supported by Retrofit55 project received funding from the European Union's Horizon Europe research and innovation program under the grant agreement No 101096068. The opinions expressed in this document reflect only the author's view and in no way reflect the European Commission's opinions. The European Commission is not responsible for any use that may be made of the information it contains.

REFERENCES

Arribas, P.F. (2007) "Some methods to obtain the added resistance of a ship advancing in waves", *Ocean Engineering*, 34, pp. 946–955.

Belibasakis, K.A, Politis, G.K. (1998) "A Non-Linear Velocity Based Boundary Element Method for the Analysis of Marine Propellers in Unsteady Flow", *Int.Shipbuilding Progress* 45, pp. 93-133.

Belibassakis K.A., Politis, G.K., Gerostathis Th.P. (2013) "Calculation of ship hydrodynamic propulsion in rough seas by non-linear BEM with application to reduction of energy losses in waves", 32th Int. Conf. on *Offshore Mech. and Arctic Engineering* (OMAE2013), June 9-14, 2013 - Nantes, France.

Belibassakis, KA, Politis, G. (2019) "Generation and propagation of noise from cavitating marine propellers", *6th Intern. Symposium on Marine Propulsors* SMP'19, Rome, Italy, May 2019.

Belibassakis KA, ES Filippas (2022) "A Dynamical System for the Combined Performance of Innovative Biomimetic Thruster With Standard Propulsion System in Waves", Int. Conference on *Offshore Mech. and Arctic Engineering* (OMAE2022), Hamburg, Germany.

Chou, T., Kosmas, V., Acciaro, M., Renken, K. (2021) "A Comeback of Wind Power in Shipping: An Economic and Operational Review on the Wind-Assisted Ship Propulsion Technology". *Sustainability* 13, 1880.

Gerritsma, J., Beukelman, W. (1972) "Analysis of the resistance increase in waves of a fast cargo ship", *International Shipbuilding Progress* 19(217), pp. 285-293.

ITTC 2002, Report of the Resistance Committee, 23rd Inter. Towing Tank Conf.

Katz J, Plotkin A. (1991) *Low speed aerodynamics.* New York: McGraw-Hill.

Kerwin, I.E., Lee, C.S. (1978) "Prediction of steady and unsteady marine propeller performance by numerical lifting-surface theory", SNAME Transactions, vol. 86.

Kinnas S. (1996) "Theory and numerical methods of hydrodynamic analysis of marine propellers", in *Advances in Marine Hydrodynamics* (Ed. M. Okhusu), Comp. Mech. Publications.

Lee, Chang-Sup (1979). Prediction of Steady and Unsteady Performance of Marine with or without Cavitation by Numerical Lifting Surface Theory, PhD Thesis. Massachusetts Institute of Technology.

Lewis, E.V. (Ed), (1989) *Principles of Naval Architecture*, vol. 3, NJ: Society Naval Architects & Marine Engin. (SNAME), New York.

Loukakis, T.A., Sclavounos, P. (1978) "Some extensions of the classical approach to strip theory of ship motion, including the calculation of mean added forces and moments", *Journal of Ship Research*, 22 (1), pp. 1–19.

Muntean T. (2008) "Ship propulsion train efficiency sensing", *Wartsila Technical Journal*, 02.2008.

Ochi, M.K. (1998). *Ocean Waves. The Stochastic Approach*, Cambridge University Press.

Papanikolaou, A.D. (2022) "Holistic Approach to Ship Design", *J. Mar. Sci. Eng.* 10, 1717.

Politis G.K. (2004) "Simulation of Unsteady motion of a propeller in a fluid including free wake modelling", *Engineering Analysis Boundary Elements*, 28(6), pp. 633-653.

Politis, G.K., Belibasakis, K.A. (1990) "Application of Panel Methods to Linearized Lifting Surface Propeller Performance Problem". Proc. *5th Int. Congress Marine Technology*, IMAEM'90. Athens, Greece.

Salvesen, N., Tuck, E.O., Faltinsen O., (1970) "Ship motions and sea loads", Transactions SNAME 78, pp 250–87.

Spinelli, F., Mancini, S., Vitiello, L., Bilandi, R.N., De Carlini, M. (2022), "Shipping Decarbonization: An Overview of the Different Stern Hydrodynamic Energy Saving Devices" *J. Mar. Sci. Eng*. 10, 574.